Letter

Crystal size dependence of dipolar ferromagnetic order between Mn_6 molecular nanomagnets

E. Burzurí,[1,2,*] M. J. Martínez-Pérez,[3] M. Muntó,[4,5] L. A. Barrios,[6] N. Ventosa,[4,5] O. Roubeau,[3] J. Veciana,[4,5] G. Aromí,[6] and F. Luis[3,†]

[1]*Departamento de Física de la Materia Condensada and Condensed Matter Physics Center (IFIMAC), Universidad Autónoma de Madrid, 28049 Madrid, Spain*

[2]*IMDEA Nanociencia, Campus de Cantoblanco, 28049 Madrid, Spain*

[3]*Instituto de Nanociencia y Materiales de Aragón (INMA), CSIC and Universidad de Zaragoza, Plaza San Francisco s/n 50009 Zaragoza, Spain*

[4]*Institut de Ciència de Materials de Barcelona (ICMAB-CSIC), Campus UAB, Cerdanyola del Vallès, Spain*

[5]*Networking Biomedical Research Networking Center on Bioengineering, Biomaterials and Nanomedicine (CIBER-BBN), Spain*

[6]*Departament de Química Inorgànica and IN2UB, Universitat de Barcelona, Martí i Franquès 1-11, 08028 Barcelona, Spain*

(Received 18 July 2022; revised 9 November 2022; accepted 14 November 2022; published 28 November 2022)

We study how crystal size influences magnetic ordering in arrays of molecular nanomagnets coupled by dipolar interactions. Compressed fluid techniques have been applied to synthesize crystals of Mn_6 molecules (spin $S = 12$) with sizes ranging from 28 μm down to 220 nm. The onset of ferromagnetic order and the spin thermalization rates have been studied by means of ac susceptibility measurements. We find that the ordered phase remains ferromagnetic, as in the bulk, but the critical temperature T_c decreases with crystal size. Simple magnetostatic energy calculations, supported by Monte Carlo simulations, account for the observed drop in T_c in terms of the minimum attainable energy for finite-sized magnetic domains limited by the crystal boundaries. Frequency-dependent susceptibility measurements give access to the spin dynamics. Although magnetic relaxation remains dominated by individual spin flips, the onset of magnetic order leads to very long spin thermalization time scales. The results show that size influences the magnetism of dipolar systems with as many as 10^{11} spins and are relevant for the interpretation of quantum simulations performed on finite lattices.

DOI: 10.1103/PhysRevB.106.L180407

Dipolar magnetic interactions are ubiquitous in nature. They lead to the formation of domains in magnetically ordered materials [1], often determine the linewidth of magnetic resonance spectra [2], and lie behind some exotic magnetic states, such as spin ice [3]. From a fundamental perspective, arrays of spins coupled solely by dipolar interactions provide close approximations of mean-field models [4] and afford the experimental observation of magnetic quantum phase transitions [5,6]. More recently, artificial spin systems coupled by long-range interactions have aroused interest within the context of quantum simulation [7,8]. Dipolar interactions can introduce unconventional dynamics in the way magnetic correlations and entanglement grow in three-dimensional spin lattices [9,10].

The ground state of a magnetic dipole crystal is one of its most basic and arguably also one of the simplest properties. In principle, the ordered phase and the phase transition must be uniquely determined by the lattice symmetry [11–13]. However, even for classical spins, the existence of dipolar ferromagnetism in real materials remained in doubt for many years. The onset of a spontaneous magnetization increases the magnetostatic energy and destabilizes the ferromagnetic phase. That a well-defined magnetic ground state exists, irrespective of the lattice shape, was rigorously proven [14]. The proof is based on the possibility of subdividing the specimen into smaller domains [15], just as in exchange-coupled ferromagnets, which retain a net spontaneous magnetization while reducing the overall magnetostatic energy. However, this prediction only works in the thermodynamic limit with an infinite (or sufficiently large) number of interacting spins. It then ensues that not only the critical temperature T_c but even the nature of the ordered phase can be quite sensitive to the lattice size when dealing with pure dipolar spin systems.

Studying this question experimentally is, however, quite challenging because real materials ordering purely by dipole-dipole interactions are scarce. Examples include some lanthanide-based compounds [16,17] and crystals of artificial magnetic molecules [18,19]. Because of the almost negligible intermolecular electronic exchange, molecular crystals can be seen as model lattices of identical magnetic dipoles. The particular system chosen for our experiments, $[Mn_6O_4Br_4(Et_2dbm)_6]$ (Et_2dbm = an ethyl para-substituted dibenzoylmethane) [20], hereafter referred to as Mn_6, is shown in Fig. 1. The symmetry of the cluster core leads to a large molecular spin $S = 12$, thus also to a large magnetic moment and sizable dipolar couplings, with a very weak magnetic anisotropy. The combination of these two properties allows the spins to order before their reversal times become too long. In bulk form, this material provides one of the

*enrique.burzuri@uam.es
†fluis@unizar.es

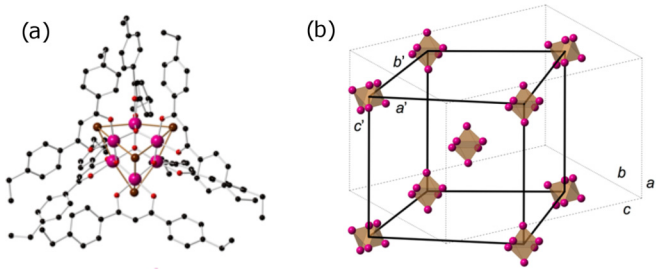

FIG. 1. (a) Structure of the $[Mn_6O_4Br_4(Et_2dbm)_6]$ molecule, highlighting the octahedron formed by the six Mn^{3+} ions (purple spheres) and the pyramid with the four Br^- ions (brown spheres) at the apices. H atoms are omitted for clarity. Color code: Mn, purple; Br, brown; O, red; and C, black. (b) Crystal lattice of Mn_6 clusters that can be approximated to a body-centered tetragonal unit cell (solid black lines). The actual monoclinic cell (see Supplemental Material [25] for details) is shown as dashed lines. For simplicity, only the central octahedron of each Mn_6 molecule is shown.

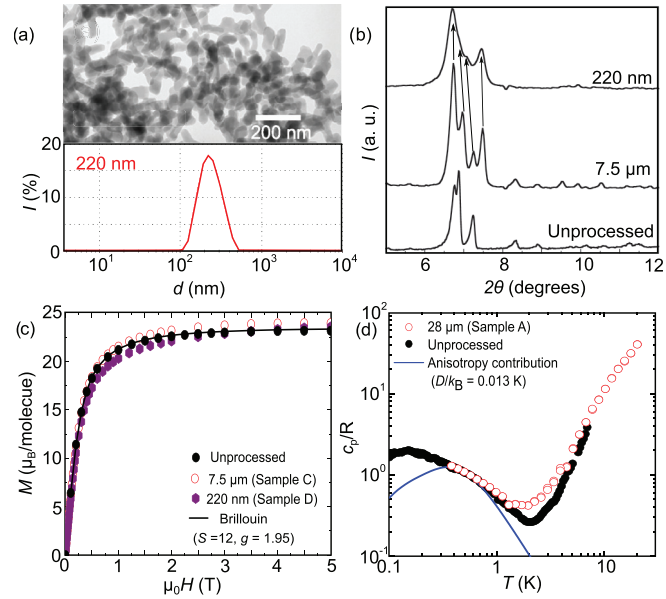

FIG. 2. (a) Transmission electron microscopy image (top) and crystal size distribution measured by dynamic light scattering (bottom) of sample D. The distribution is centered at 220 nm with a half width at half maximum of 75 nm. (b) X-ray diffraction spectra measured on a powder sample of unprocessed bulk Mn_6 and on samples C and D having average crystal sizes of 7.5 μm and 220 nm, respectively. (c) Magnetization isotherms measured on unprocessed Mn_6 and on the same C and D samples. The fit with a Brillouin function (solid line) gives $S = 12$ and $g = 1.95$. (d) Molar specific heat of unprocessed Mn_6 and of sample A measured at zero field as a function of temperature. The solid line shows the Schottky contribution due to the magnetic anisotropy of each molecule. In both cases, the results are compatible with a weak uniaxial anisotropy constant $D/k_B = 0.013$ K [21,22].

cleanest examples of pure dipolar ferromagnetism with $T_c \simeq 0.16$ K [21,22]. A last necessary ingredient is the ability to control crystal size while preserving other relevant properties, something that often lies beyond the capabilities of conventional synthetic methods. A promising way to improve the control and homogeneity is provided by recrystallization in supercritical fluids [23,24].

Here, we study the magnetic ordering in micro- and nanocrystals of Mn_6. By means of ac susceptibility measurements, we investigate the phase transition as a function of crystal size and the spin relaxation toward thermal equilibrium. The results are analyzed based on ground state energy calculations and Monte Carlo simulations that consider how the lattice size affects dipolar interactions.

The starting material, unprocessed bulk Mn_6, was synthesized following the method reported in Ref. [20] and characterized as described in the Supplemental Material [25] (see, also, Refs. [26–29] therein). Crystals of varying size were obtained by recrystallization in compressed supercritical fluids via two techniques: the gas antisolvent (GAS) method and the aerosol solvent extraction system (ASES) method. Details of these methods can be found elsewhere [23]. Samples of Mn_6 crystals with average lengths (A) 28 μm, (B) 12 μm, and (C) 7.5 μm were prepared using the GAS method. The smallest particles, with an average size of 220 nm, were prepared with the ASES method (sample D). Transmission electron microscopy [Fig. 2(a)] shows the tendency of Mn_6 to grow in elongated shapes. The size distribution of each set of crystals was measured using dynamic light scattering, providing evidence for rather narrow distributions, as shown in Fig. 2(a) for sample D (see Supplemental Material [25] for information on the other samples).

The samples were characterized by different techniques to determine how the structural and magnetic properties of Mn_6 are modified by the recrystallization process. Single-crystal synchrotron diffraction experiments have allowed us to verify that all four samples remain (poly-)crystalline and to derive the unit cell for various crystals of sample C (see Supplemental Material [25] and Refs. [26–29] therein for more details). The cell parameters remain very similar to those of bulk Mn_6 although with departures from strict monoclinic symmetry, i.e., angles tending to deviate from 90° and a variation <4% in the cell volume. Additional x-ray powder diffraction experiments were performed on all samples. The patterns for unprocessed bulk Mn_6 and samples C and D are compared in Fig. 2(b). A significant broadening of the main peaks is observed in the case of sample D that can be ascribed to the significantly reduced size of the crystallites. This broadening likely impedes the detection of weaker peaks at higher angles. In addition to this, the diffraction patterns remain very similar upon reducing crystal size, but they show some differences with respect to that of the original unprocessed material. This is relevant for pure dipolar systems where the magnetic ground state is mainly determined by the lattice geometry [11].

The magnetic properties of Mn_6 can be described with the following spin Hamiltonian [21,22]:

$$\mathcal{H} = -\sum_{i=1}^{N}\left(DS_{i,z}^2 + g\mu_B\vec{B}\vec{S}_i\right) + g^2\mu_B^2\sum_{i\neq j}\left[\frac{\vec{S}_i\vec{S}_j}{r_{ij}^3} - \frac{3(\vec{S}_i\vec{r}_{ij})(\vec{S}_j\vec{r}_{ij})}{r_{ij}^5}\right], \quad (1)$$

where the first term is a uniaxial magnetic anisotropy, the second describes the Zeeman interaction of the molecular magnetic moment $\vec{\mu} = g\mu_B\vec{S}$ with magnetic field $\vec{B}$, and the third accounts for the dipolar interactions between different molecules. Figure 2(c) shows the magnetization M measured as a function of B for the original Mn_6 and for samples C and D. In this temperature range, anisotropy and dipolar couplings play a negligible role; thus, the molecular spin S and the g factor can be determined by fitting M with a Brillouin function (see also the Supplemental Material [25]). We obtain $S = 12$ and $g = 1.95$, in good agreement with those previously found in the bulk [21]. Figure 2(d) compares the specific heat c_p of sample A measured down to 300 mK with that of unprocessed Mn_6 [21]. The magnetic contribution, which becomes dominant $<\sim 2$ K, is the same in the temperature range common to both measurements. The solid line shows the Schottky contribution associated with the magnetic anisotropy. It follows that the anisotropy constant remains virtually the same as in the starting material $D/k_B \simeq 0.013$ K [20]. From these results, we conclude that recrystallization in compressed fluids largely preserves all relevant molecular properties and that it gives rise to a well-defined crystal lattice. These Mn_6 crystallites provide therefore a model system to study how crystal size affects long-range dipolar ordering.

The complex ac susceptibility $\chi(\omega, T) = \chi'(\omega, T) - i\chi''(\omega, T)$, where ω is the ac frequency, was measured with a microsuperconducting quantum interference device (μSQUID) susceptometer [30,31] immersed inside the mixing chamber of a ^{3}He - ^{4}He dilution refrigerator to maximize the thermal exchange between the sample, helium bath, and thermometer. A small amount of crystalline powder was mixed with a nonmagnetic grease and directly deposited onto the μSQUID susceptometer. The measurements were performed in the frequency range 15 mHz $< \omega/2\pi <$ 130 kHz and for temperatures ranging between 45 mK and 20 K. More details about this measuring technique are given in the Supplemental Material [25].

Figure 3(a) shows the in-phase component χ' measured for sample A at different frequencies. The susceptibility shows a paramagnetic response $\chi' \propto 1/(T - \theta)$ interrupted by a frequency-dependent peak. The temperature of the maximum decreases with ω following the Arrhenius law [Fig. 3(c)]. In this paramagnetic regime, the spin dynamics can be understood on a quite simple basis, characteristic of many single-molecule magnets: the magnetic anisotropy of each cluster generates an energy barrier $U = DS^2 \simeq 1.87$ K for the reversal of its spin, which slows down spin thermalization exponentially as T decreases. This means that progressively lower frequencies are needed to explore the equilibrium magnetic response at lower temperatures. Interestingly, for $\omega/2\pi < 0.1$ Hz, the peak becomes approximately independent of frequency which, in analogy with what was observed for unprocessed Mn_6, we assign to the onset of a magnetically ordered phase. The maximum $\chi' \simeq 0.16$ emu/g is close to the ferromagnetic limit, determined by the demagnetizing factor [22] and marked as a dashed horizontal line in Fig. 3(a). The intrinsic reciprocal susceptibility, corrected for demagnetization effects [Fig. 3(d)], follows the Curie-Weiss law, with a positive Weiss temperature θ, as expected for mean-field-like dipolar ferromagnets [4]. Therefore, we conclude that magnetic order remains ferromagnetic, albeit the critical temperature $T_c \simeq 0.121$ K, extracted from the position of the susceptibility maximum, turns out to be lower than $T_c \simeq 0.16$ K of the unprocessed Mn_6 [21,22]. The difference might be associated with their slightly different crystal lattices [see Fig. 2(b)]. For this reason, in the discussion that follows sample A will be used as the reference bulk limit.

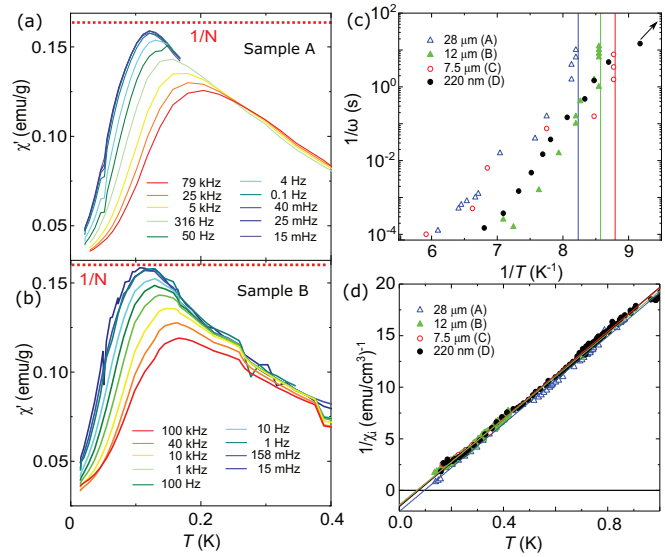

FIG. 3. (a) In-phase magnetic susceptibility χ' of sample A (average crystal size 28 μm) measured as a function of temperature for different frequencies $\omega/2\pi$ ranging from 15 mHz (blue) to 79 kHz (red). The maximum χ' becomes independent of ω <0.1 Hz and saturates at a value close to $1/\rho N = 0.16$ emu/g (dotted red line), signaling the onset of ferromagnetic order. (b) Same as in (a) for sample B (average crystal size 12 μm). (c) Arrhenius plot for the frequency-dependent temperature of maximum χ'. The tendency of this temperature to saturate to a constant value points to a magnetic phase transition and provides a method to estimate the critical temperature T_c (vertical solid lines). (d) Reciprocal equilibrium susceptibility of all samples, corrected from demagnetizing effects, as a function of temperature. The solid lines are least squares Curie-Weiss fits.

We next consider the change in T_c with crystal size. For this, we compare results obtained for samples B–D by the same method outlined above to the value found for sample A. The susceptibility of sample B (12 μm) is shown in Fig. 3(b), while those of samples C and D can be found in the accompanying Supplemental Material [25]. The frequency-independent susceptibility peak shifts to lower temperatures with decreasing size, $T_c \simeq 0.114$ K for sample B (12 μm) and $\lesssim$0.11 K for sample C (7.5 μm). For sample D, which contains the smallest crystals (220 nm), it is not observed even for frequencies as low as 15 mHz, which sets $T_c < 0.1$ K.

These T_c values, normalized to that found for sample A, are plotted in Fig. 4(a) as a function of average particle size d. The physics underlying the decrease in T_c can be understood by considering the dipolar energies of ferromagnetic domains polarized along the magnetic anisotropy axis z. To simplify the analysis, the Mn_6 lattice was approximated to a body-centered tetragonal lattice with $a' = b' = 18.0$ Å and $c' = 17.7$ Å [see Fig. 1(b) and the inset of Fig. 4(b)].

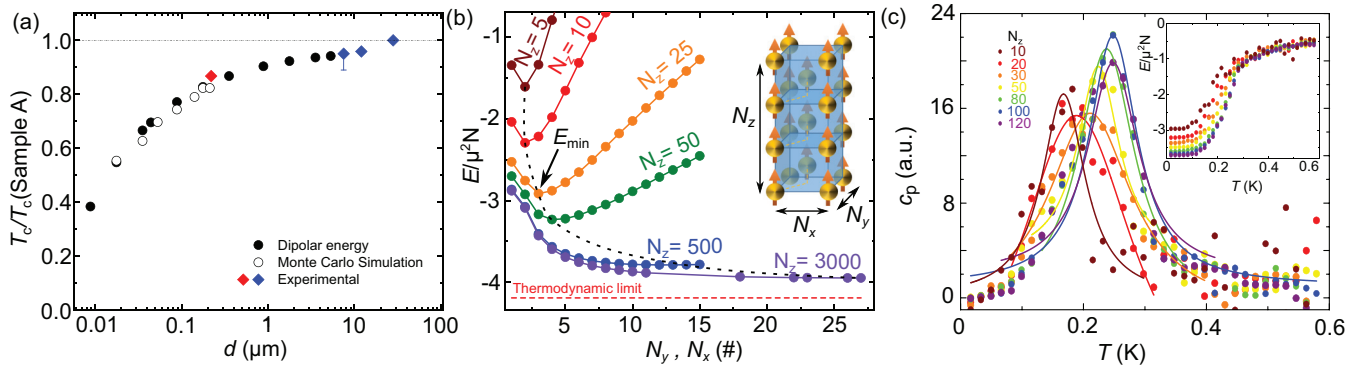

FIG. 4. (a) Critical temperature of Mn_6 molecular crystals, estimated from ac susceptibility measurements and normalized to T_c of sample A (solid rhombic dots), as a function of average crystal size d. The plot also shows dipolar energies of ferromagnetic domains [solid circles, see (b)] and critical temperatures determined from Monte Carlo simulations [open circles, see (c)], in both cases normalized to the bulk values. (b) Dipolar energy E of ferromagnetic domains with different lengths N_z as a function of domain width $N_x = N_y$. The dotted line marks the minimum dipolar energy E_{min} attainable for each domain size. The inset shows an scheme of the tetragonal lattice used in these energy calculations and in the Monte Carlo simulations, where N_x, N_y, and N_z denote number of sites. (c) Magnetic heat capacity obtained from Monte Carlo simulations on lattices of varying N_z and fixed $N_x = N_y = 5$ sites. The solid lines are least squares fits to Lorentzian curves that allow finding T_c. The inset shows the dipolar energy as a function of temperature from which the specific heat curves are derived.

Figure 4(b) shows that a domain of length N_z attains a minimum energy for a width $N_x = N_y < N_z$ that gives a sufficiently low demagnetizing factor. The minimum attainable energy E_{min} reflects the number of interacting spins in the domain, and it is therefore limited by size, decreasing toward its thermodynamic limit [11], $E = -(4\pi/3)N\mu^2$ with $N = 2N_xN_yN_z$, as N_z increases. The critical temperature measures the strength of thermal fluctuations needed to break magnetic order; thus, it also decreases with increasing size. The link between E_{min} and T_c has been tested by means of Monte Carlo simulations performed on the same lattice yet necessarily of a smaller size. We fixed $N_x = N_y = 5$ sites, while N_z was varied between 10 and 120, which approximately corresponds to 20–200 nm. Initially, spins are randomly pointing up or down at high T. Then the temperature of the simulation is decreased, and the energies of the different configurations are computed with Eq. (1). Results are shown in Fig. 4(c). A steplike drop in energy is observed, which marks a transition to the ferromagnetic phase. As expected, the minimum attainable energy in this state decreases with increasing N_z. The size-dependent T_c can be determined from the specific heat maximum and follows a similar trend. The results obtained from both methods are included in Fig. 4(a). They account fairly well for the observed decrease in T_c.

It follows that crystal size begins to influence long-range dipolar order for remarkably large lattices (with as many as 10^{11} spins in the case of sample B). This contrasts with predictions for short-range interactions [32] and with results observed in thin magnetic films [33]. In this case, T_c decreases mainly from the reduced coordination of spins located near the surface; thus, it becomes noticeable only when its fraction becomes sufficiently high. As discussed above, the situation is different with dipolar spin lattices, for which the minimum dipolar energy becomes a compromise between the net interaction field felt by each spin and the demagnetizing factor. Because of the slow decay of dipolar interactions with size and the increasing number of neighbors at any given increasing distance, the surface of the sample is not the determinant factor. All spins, including those at the core are affected by limitations that crystal boundaries impose on the domain size. This explains why the minimum domain energy and T_c start to feel the reduction in the number of spins at such large lattice sizes.

Finally, we focus on the dynamics of the spin system by looking at the frequency dependence of the linear response (Fig. 5). For a variety of magnetic systems, this dependence can be understood based on the Cole-Cole equation for the complex ac susceptibility [34]:

$$\chi(\omega, T) = \chi_S + \frac{\chi_T - \chi_S}{1 + i(\omega\tau)^{1-\alpha}}, \tag{2}$$

where χ_S and χ_T are the adiabatic (infinite-frequency) and isothermal (equilibrium or zero-frequency) susceptibility limits, respectively, τ is an average spin-relaxation time, and $0 \leqslant \alpha \leqslant 1$ parameterizes the relaxation time distribution ($\alpha = 0$ corresponds to a system with a single τ, and the distribution broadens as α approaches unity). Whenever the out-of-phase susceptibility component χ'' becomes maximum, $1/\omega$ provides a measure of the dominant relaxation time. Figure 5(a) shows χ'' of sample A at 10 different frequencies from 15 mHz up to 79.4 kHz. Its maximum shifts to lower temperature as ω decreases, following an Arrhenius law $1/\omega = \exp(U/k_BT)$ for $T > 60$ mK and then leveling off a little. The activation energy $U/k_B \simeq 1.4(1)$ K for samples A–C and 1.6(1) K for sample D. This is close to the anisotropy barrier for a single molecular spin. The saturation observed at very low T shows that thermal activation is gradually replaced by temperature-independent spin-tunneling processes [35–38]. These results therefore suggest that the spin thermalization remains dominated by single spin flips even well into the ferromagnetic phase. This is understandable, considering the weak dipolar interaction strength as compared with the magnetic anisotropy, which allows magnetic domain walls to move by reversing a spin at a time without incurring a too-high energy cost [1].

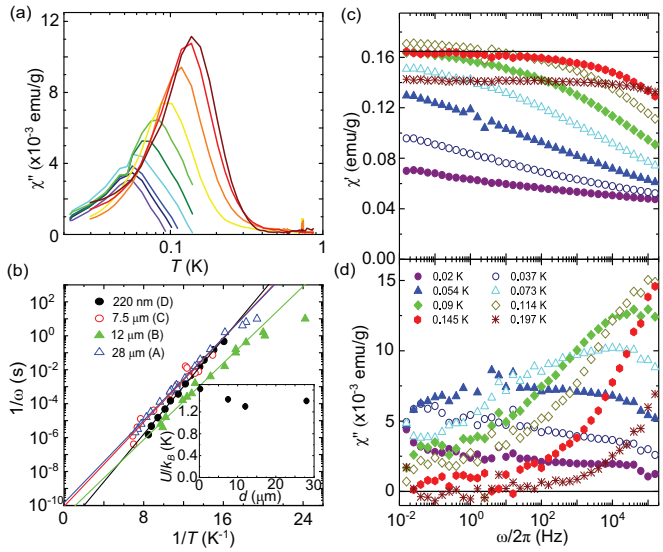

FIG. 5. (a) Out-of-phase magnetic susceptibility component χ'' of sample A (average crystal size 28 μm) measured as a function of temperature at 10 different frequencies spanning eight decades, from 79.433 kHz (dark red) to 15.85 mHz (purple). (b) Arrhenius plots for the frequency-dependent temperatures of maximum χ'' for all samples. This plot provides information on the temperature dependence of the typical spin thermalization times. Solid lines are least square Arrhenius fits $1/\omega = \tau_0 \exp(U/k_B T)$, with τ_0 an attempt time and U the activation energy. The inset shows U as a function of average crystal size. (c) Isotherms of χ' (top) and χ'' (bottom) of sample B as a function of frequency for temperatures across $T_c \simeq 0.114$ K. Notice the sudden broadening of these curves that occurs at and below T_c.

Still, some features indicate that magnetic order does affect the spin dynamics near and below T_c. The maximum χ'' decreases with temperature [Fig. 5(a)]. According to Eq. (2) and considering that the equilibrium ferromagnetic $\chi_T \simeq 1/N$, it follows that the relaxation time distribution broadens below T_c. This can be seen directly by looking at the frequency-dependent susceptibility measured at fixed temperatures [Figs. 5(c) and 5(d)]. As T_c is approached from above, χ'' develops a low-frequency tail, signaling the onset of very slow thermalization processes, with characteristic timescales longer than seconds. These are probably associated with the stabilization of certain domain configurations by the growth of magnetic correlations. Incidentally, this explains why the onset of magnetic order gives rise to a maximum in χ' and not a plateau and provides a dynamic signature for detecting the phase transition (e.g., by monitoring χ'' measured at the lowest attainable frequency). For sample D, the broadening starts ∼100 mK (see Supplemental Material [25]), which suggests that T_c is not too far below this temperature.

In conclusion, we have exploited recrystallization in supercritical fluids to grow molecular crystals of decreasing size and to explore how this affects magnetic order in a model dipolar lattice. The results show that, while the ordered phase remains the same (in our case, ferromagnetic), there is a drop in the transition temperature T_c. Finite-sized effects in this system become already noticeable for lattice sizes of a few microns, equivalent to a spin number $N > 10^{11}$, thus are stronger than those predicted and observed for magnetic systems with dominant short-range spin-spin interactions. This effect ensues as a consequence of the slow decrease of dipolar interactions with distance. In addition, we have observed that, even though the spin relaxation remains dominated by single spin flips, the growth of spin correlations introduces very long spin thermalization times. In addition to providing direct evidence on some of the fundamental properties of dipolar magnets, these results might also have a relevance for the interpretation of experiments performed on other systems characterized by dominant long-range interactions. The connection between the ground states obtained for necessarily small-scale quantum simulators [7,8] and predictions for real phases in quantum magnets must be done with some caution and consider finite-sized effects. On the other hand, the relative frailty of spin systems coupled by dipolar interactions also makes them of interest for the implementation of proposals to modify and control magnetic order via the interaction to photons in superconducting circuits [39].

We acknowledge support from Grants No. RTI2018-096075-B-C21 and No. RTI2018-096075-A-C22, funded by MCIN/AEI/10.13039/501100011033 and ERDF A way of making Europe, Grant No. RYC2019-028429-I, funded by MCIN/AEI/10.13039/501100011033 and ESF Investing in your future, the Gobierno de Aragón Grant No. E09-20R-Q-MAD, and the CSIC Quantum Technology Platform PT-001. This letter used resources of the Advanced Light Source, a Department of Energy, Office of Science User Facility under Contract No. DEAC02-05CH11231. The synthesis and size measurements of Mn_6 micro- and nanocrystals were done at the U6 unit of NANBIOSIS ICTS, located at the Institute of Materials Science of Barcelona (CSIC).

[1] C. Kittel, Rev. Mod. Phys. **21**, 541 (1949).
[2] J. H. Van Vleck, Phys. Rev. **74**, 1168 (1948).
[3] B. C. den Hertog and M. J. P. Gingras, Phys. Rev. Lett. **84**, 3430 (2000).
[4] A. Aharony, Phys. Rev. B **8**, 3363 (1973).
[5] D. Bitko, T. F. Rosenbaum, and G. Aeppli, Phys. Rev. Lett. **77**, 940 (1996).
[6] E. Burzurí, F. Luis, B. Barbara, R. Ballou, E. Ressouche, O. Montero, J. Campo, and S. Maegawa, Phys. Rev. Lett. **107**, 097203 (2011).
[7] P. Richerme, C. Senko, S. Korenblit, J. Smith, A. Lee, R. Islam, W. C. Campbell, and C. Monroe, Phys. Rev. Lett. **111**, 100506 (2013).
[8] R. Islam, C. Senko, W. C. Campbell, S. Korenblit, J. Smith, A. Lee, E. E. Edwards, C.-C. J. Wang, J. K. Freericks, and C. Monroe, Science **340**, 583 (2013).
[9] J. Eisert, M. van den Worm, S. R. Manmana, and M. Kastner, Phys. Rev. Lett. **111**, 260401 (2013).
[10] J. Schachenmayer, B. P. Lanyon, C. F. Roos, and A. J. Daley, Phys. Rev. X **3**, 031015 (2013).

[11] J. M. Luttinger and L. Tisza, Phys. Rev. **70**, 954 (1946).
[12] T. Niemeijer and H. Blöte, Physica **67**, 125 (1973).
[13] S. K. Misra, Phys. Rev. B **14**, 5065 (1976).
[14] R. B. Griffiths, Phys. Rev. **176**, 655 (1968).
[15] C. Kittel, Phys. Rev. **82**, 965 (1951).
[16] M. R. Roser and L. R. Corruccini, Phys. Rev. Lett. **65**, 1064 (1990).
[17] M. R. Roser, J. Xu, S. J. White, and L. R. Corruccini, Phys. Rev. B **45**, 12337 (1992).
[18] D. Gatteschi, R. Sessoli, and J. Villain, *Molecular Nanomagnets* (Oxford University Press, Oxford, 2006).
[19] J. Bartolomé, F. Luis, and J. F. Fernández, *Molecular Magnets, Physics and Applications* (Springer, Berlin, Heidelberg, 2014).
[20] G. Aromí, M. J. Knapp, J.-P. Claude, J. C. Huffman, D. N. Hendrickson, and G. Christou, J. Am. Chem. Soc. **121**, 5489 (1999).
[21] A. Morello, F. L. Mettes, F. Luis, J. F. Fernández, J. Krzystek, G. Aromí, G. Christou, and L. J. de Jongh, Phys. Rev. Lett. **90**, 017206 (2003).
[22] A. Morello, F. L. Mettes, O. N. Bakharev, H. B. Brom, L. J. de Jongh, F. Luis, J. F. Fernández, and G. Aromí, Phys. Rev. B **73**, 134406 (2006).
[23] M. Muntó, J. Gómez-Segura, J. Campo, M. Nakano, N. Ventosa, D. Ruiz-Molina, and J. Veciana, J. Mater. Chem. **16**, 2612 (2006).
[24] N. Domingo, F. Luis, M. Nakano, M. Muntó, J. Gómez, J. Chaboy, N. Ventosa, J. Campo, J. Veciana, and D. Ruiz-Molina, Phys. Rev. B **79**, 214404 (2009).
[25] See Supplemental Material at http://link.aps.org/supplemental/10.1103/PhysRevB.106.L180407 for details on the synthesis and structural characterization of the different samples, additional magnetization and susceptibility data, and a description of the theoretical study of dipolar interactions.
[26] L. Krause, R. Herbst-Irmer, G. M. Sheldrick, and D. Stalke, J. Appl. Cryst. **48**, 3 (2015).
[27] G. M. Sheldrick, Acta Cryst. A **64**, 112 (2008).
[28] G. M. Sheldrick, Acta Cryst. C **71**, 3 (2015).
[29] A. L. Spek, Acta Cryst. C **71**, 9 (2015).
[30] M. J. Martínez-Pérez, J. Sesé, F. Luis, D. Drung, and T. Schurig, Rev. Sci. Instrum. **81**, 016108 (2010).
[31] M. J. Martínez-Pérez, J. Sesé, F. Luis, R. Córdoba, D. Drung, T. Schurig, E. Bellido, R. de Miguel, C. Gómez-Moreno, A. Lostao *et al.*, Trans. Appl. Supercond. **21**, 345 (2011).
[32] D. P. Landau, Phys. Rev. B **14**, 255 (1976).
[33] M. Farle, K. Baberschke, U. Stetter, A. Aspelmeier, and F. Gerhardter, Phys. Rev. B **47**, 11571 (1993).
[34] K. S. Cole and R. H. Cole, J. Chem. Phys. **9**, 341 (1941).
[35] C. Sangregorio, T. Ohm, C. Paulsen, R. Sessoli, and D. Gatteschi, Phys. Rev. Lett. **78**, 4645 (1997).
[36] N. V. Prokof'ev and P. C. E. Stamp, Phys. Rev. Lett. **80**, 5794 (1998).
[37] J. F. Fernández, Phys. Rev. B **66**, 064423 (2002).
[38] F. Luis, M. J. Martínez-Pérez, O. Montero, E. Coronado, S. Cardona-Serra, C. Martí-Gastaldo, J. M. Clemente-Juan, J. Sesé, D. Drung, and T. Schurig, Phys. Rev. B **82**, 060403(R) (2010).
[39] J. Román-Roche, F. Luis, and D. Zueco, Phys. Rev. Lett. **127**, 167201 (2021).